BIOCHEMISTRY
including biophysical chemistry & molecular biology

Article

pubs.acs.org/biochemistry

A Host−Guest Relationship in Bone Morphogenetic Protein Receptor-II Defines Specificity in Ligand−Receptor Recognition

Lee-Chuan C. Yeh,[†] Wilfredo E. Falcon,[‡] Andrea Garces,[‡] J. Ching Lee,[‡] and John C. Lee*,[†]

[†]Department of Biochemistry, University of Texas Health Science Center at San Antonio, San Antonio, Texas 78229, United States
[‡]Department of Biochemistry and Molecular Biology, University of Texas Medical Branch, Galveston, Texas 77555, United States

Supporting Information

ABSTRACT: One of the most intriguing questions confronting the bone morphogenetic protein family is the mechanism of ligand recognition, because there are more ligands than receptors. Crystal structures of two type II receptors, ActR-II and BMPR-II, are essentially identical, and a loop structure (A-loop) has been suggested to play a role in determining ligand specificity. A solution biophysical study showed mutations of several A-loop residues in these two receptors exert different ligand binding effects. Thus, the issues of mechanism of ligand recognition and specificity remain unresolved. We examined effects of mutations of residues Y40, G47, and S107 in BMPR-II. These residues are not identified as being in contact with the ligand in the BMP-7−BMPR-II complex but are found mutated in genetic diseases. They are likely to be useful in identifying their roles in differentiating the various BMP ligands. Spectroscopic probing revealed little mutation-induced structural change in BMPR-II. Ligand binding studies revealed that Y40 plays a significant role in differentiating three distinct ligands; G47 and S107 affect ligand binding to a lesser extent. The role of the A-loop in ActR-II or BMPR-II is dependent on the host sequence of the receptor extracellular domain (ECD) in which it is embedded, suggesting a host−guest relationship between the A-loop and the rest of the ECD. Computational analysis demonstrated a long-range connectivity between Y40, G47, and S107 and other locations in BMPR-II. An integration of these results on functional energetics and protein structures clearly demonstrates, for the first time, an intradomain communication network within BMPR-II.

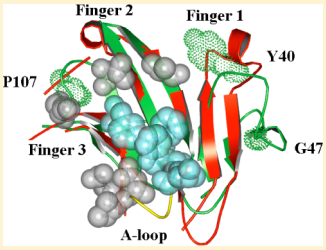

Activins (Acts) and bone morphogenetic proteins (BMPs) are members of the transforming growth factor-β (TGF-β) superfamily[1−3] and are multifunctional proteins, playing key roles in numerous biological processes, such as embryonic development, cell differentiation, proliferation, morphogenesis, tissue repair, homeostasis, and apoptosis.[4−6] On the basis of the extent of their amino acid sequence homology, numerous BMPs have been identified and classified into six subfamilies. BMPs exert their effects on cells by forming a complex with the extracellular domains (ECDs) of two different types of serine/threonine kinase receptors, known as type I and type II.[7−9] Four mammalian type I and three type II receptors have been shown to bind BMPs.[10] Because there are multiple ligands and receptors, one of the most intriguing questions confronting this system is the mechanism of ligand recognition and the structural insights into the mechanism. Studies of ligand−receptor complexes have identified protein regions and amino acid residues in the receptor essential for ligand binding.[11−16] Structures of more than a dozen receptor−ligand complexes in the TGF-β superfamily have been determined at atomic resolution.[11,13−21] In brief, these studies have shown that the ECD of the type I receptors contains two β-sheets and an α-helix organized around five disulfide bonds, and the ECD of the type II receptors contains three two-stranded β-sheets (three-finger toxin fold) also organized around five disulfide bonds.[22,23] These studies have revealed that the free receptors have a similar overall backbone fold (see Figure 1) and further suggested that the different BMPs bind to the same overall ligand binding domain without inducing significant structural

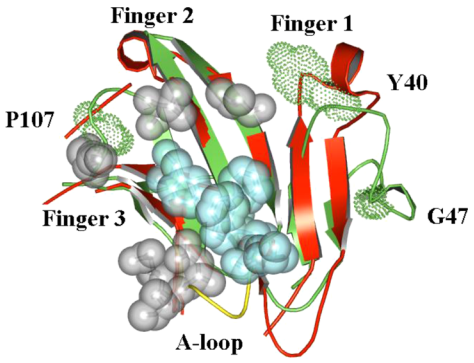

Figure 1. Alignment of the structures of ActR-II (PDB entry 1LX5, red) and BMPR-II (PDB entry 2HLQ, green). The locations of natural single-site mutants are marked as green dots, while gray spheres represent contact sites in the receptor within 4 Å of BMP-7 in a BMP−ActR-II complex (PDB entry 1LX5). The hydrophobic patch of the ligand interface is marked as cyan spheres in the bottom part of Finger 2. The A-loop is indicated and is located at the bottom of the structure.

Received: March 2, 2012
Revised: August 15, 2012
Published: August 15, 2012

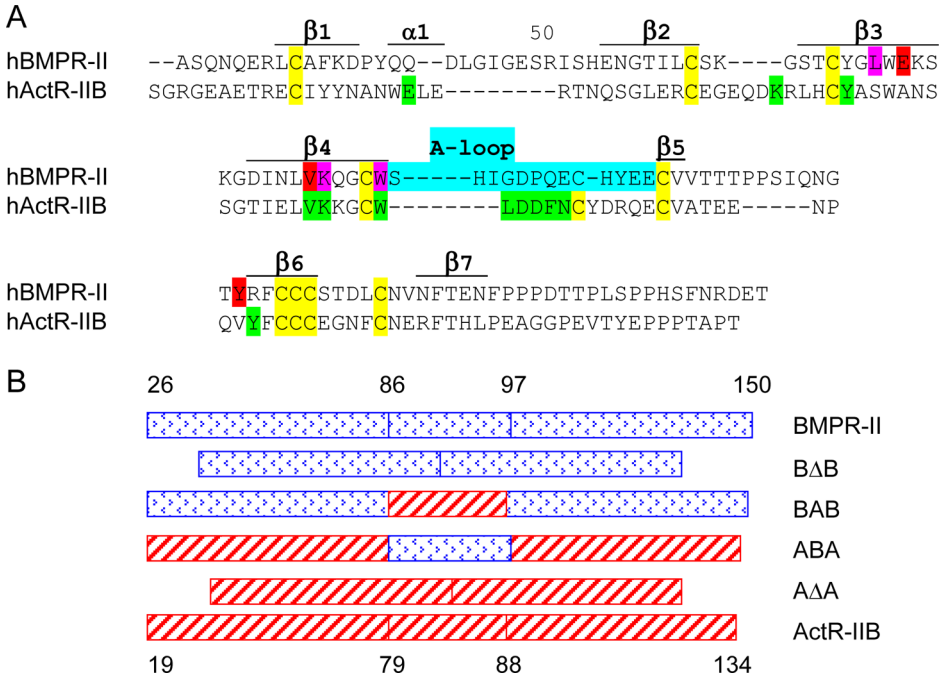

Figure 2. (A) Sequence alignment of human ActR-IIB and BMPR-II. The secondary structure ($\beta1-\beta7$) indicated atop the sequence was adopted from Greenwald et al.[22] Amino acid residues in ActR-IIB that have been shown by mutagenesis and analysis of crystal structures of ligand−receptor complexes to be important for ligand binding are colored light green.[11,16,18] Amino acid residues that have been shown by mutagenesis to be critical for ligand binding and are ligand specificity determinants are colored red and magenta, respectively.[24] (B) Schematics of chimera constructs of ActR-IIB and BMPR-II. Numbers represent amino acid residue positions. BΔB is the BMPR-II with its A-loop deleted. BAB is the chimera of BMPR-II containing the ActR-IIB A-loop. ABA is the chimera of ActR-IIB containing the BMPR-II A-loop. AΔA is ActR-IIB with its A-loop deleted.

changes. Ligands are always bound to the concave surface of the receptor ECD. The hydrophobic residues in finger 2 are always intimately involved as the binding interface (Figure 1). However, there are still incongruous conclusions derived from structural and solution studies. For example, there is disagreement about the role of specific residues or structural elements such as the loops in the receptor in determining ligand specificity.[12,24]

The goal of this study is to compare and contrast BMPR-II and ActR-II whose ECDs have essentially the same fold, although their sequences are only 24% identical. Although the apo structures of BMPR-II and ActR-II are known, the structure of the BMP-7−ActR-II complex is the only holo structure known for these two receptors. We utilized four strategies to identify the structural elements and molecular mechanism of ligand recognition. First, we included mutations identified in genetic diseases to perturb the structure of BMPR-II, assuming that these sites are important, because mutations lead to disease states. Recent discoveries of mutations in BMPR-II in patients with different diseases, including pulmonary veno-occlusive disease, congenital heart disease, and pulmonary arterial hypertension, have provided a clue about amino acid residues that might play a role in the structure and function of the receptor.[25−29] Thus, these naturally occurring mutations identified in genetic diseases in BMPR-II are expected to serve as excellent models for elucidating the role of these structural elements in this three-finger toxin fold. Second, we focused on the role of the A-loop in BMPR-II and in closely related ActR-II.[11,13−16,24] Although the primary structures of BMPR-II and ActR-II are different (Figure 2A), the three-dimensional folds are very similar as shown in the superimposed model of the two structures (Figure 1). Our strategy is to study the A-loop deletion type II receptors and chimeric type II receptor molecules with substitution of the A-loop region (Figure 2B). Third, we employed a structure-based computation algorithm, COREX/BEST, to probe the structural connectivity among various regions of the BMPR-II ECD to provide a rationale for the structure−function relationship of these mutants. Fourth, we employed the Autodock algorithm to identify potential contact residues in the ligand−BMPR-II ECD interface.

Results of these studies revealed communications among the loops and other structural domains in these receptors. The structure-based computation algorithm revealed a network of connectivity among various structural elements. Such a network could serve as an important rationale for the differentiation of the various ligands by different receptors. The network may also serve as the molecular vehicle for implementing the message imparted by the different ligands for further execution of downstream biological activities.

MATERIALS AND METHODS

Materials. All reagents were of molecular biology grade. Activin was purchased from R&D Systems (Minneapolis, MN). BMP-7 and GDF-5 were provided by Stryker Biotech (Hopkinton, MA) and were dissolved in filtered deionized, distilled water. Oligonucleotide primers were synthesized by the Advanced Nucleic Acids Core Facility of The University of Texas Health Science Center at San Antonio. Thrombin and competent *Escherichia coli* strain BL21(DE3) cells were purchased from Novagen (Madison, WI). Ni-NTA resin was purchased from Qiagen (Valencia, CA). The Superdex 200 column and C18 column were purchased from Amersham (Piscataway, NJ). Bis-ANS was purchased from Molecular Probes (Eugene, OR) and was dissolved in dimethylformamide to make a 10 mM stock. Prior to use, the bis-ANS stock

dx.doi.org/10.1021/bi3003023 | *Biochemistry* 2012, 51, 6968−6980

solution was diluted with RDB buffer [50 mM Tris-HCl (pH 7.5) and 150 mM NaCl].

Cloning and Mutagenesis. The human recombinant BMPR-II ECD sequence, corresponding to nucleotides 76−450 downstream from the translation start codon ATG (A is +1), was cloned into a modified pET32 (ΔKpn) vector as previously described.[24,30] The human recombinant ActR-IIB ECD sequence, corresponding to nucleotides 55−402 downstream from the translation start codon ATG (A is +1), was also cloned into the same vector. Desired mutants were constructed using the QuikChange site-directed mutagenesis kit (Stratagene, La Jolla, CA). Locations of these mutation sites are shown in Figure 1. Schematics of chimeric constructs of the ECD of ActR-IIB and BMPR-II are shown in Figure 2B. Each mutant plasmid was characterized by restriction enzyme mapping and double-stranded DNA sequencing to be certain that no inadvertent changes had been made.

Protein Expression and Purification. Both BMPR-II and ActR-II proteins were expressed in *E. coli* and purified to homogeneity as previously reported.[24,30] Briefly, *E. coli* BL21(DE3) cells containing these DNA clones were grown, and protein expression was induced with 0.2 mM IPTG for 3 h. All ECD proteins were expressed as a fusion protein with an N-terminal TRX sequence and a C-terminal hexahistidine tag. The TRX−ActR-IIB fusion protein and TRX−BMPR-II ECD contained 262 and 271 amino acid residues with theoretical molecular masses of 29 and 30 kDa, respectively. The fusion protein was first purified by Ni-NTA affinity chromatography and digested with thrombin. The resulting free receptor was separated from the TRX protein by Ni-NTA affinity chromatography followed by Superdex 200 gel filtration column chromatography. The monomeric receptor ECD was further purified to homogeneity with a C18 reverse phase column. The purified ActR-IIB and BMPR-II ECD contained 133 and 142 amino acid residues with theoretical molecular masses of 15 and 16 kDa, respectively. Protein concentrations were determined by the absorbance at 280 nm using a Nanodrop 1000 (Thermo Scientific, Waltham, MA). The purity of the protein was analyzed on a Tricine SDS gel. Protein samples were stored at −80 °C until they were used.

Osteocalcin Promoter−Luciferase (OC promoter−Luc) Reporter Activity Assay. The in vivo biological activity of BMPR-II mutant receptor ECDs was tested. Fetal rat calvaria (FRC) cells were cultured in a 24-well plate with αMEM and 10% FBS and transfected with FuGENE 6 (Roche, Indianapolis, IN) according to the instructions provided by the manufacturer. Briefly, the OC promoter−Luc reporter DNA complex was prepared by incubation with FuGENE 6 for 30 min at room temperature. FRC cells were rinsed with HBSS and mixed with 0.2 mL of OPTI medium and 8 units of Hyaluronidase. The DNA complex was added dropwise to the cells. After 5 h, fresh αMEM/10% FBS medium was added and incubated overnight. Transfected cells were treated with 6 nM BMP-7 in the absence or presence of a 20-fold molar excess of wild-type or mutant soluble BMPR-II for 24 h. The OC promoter activity in the cell lysate was measured by the luciferase activity using the Dual-Light System (Applied Biosystems, Foster City, CA).

Ligand Binding Activity Determined by Surface Plasmon Resonance (SPR). The ability of the different receptors to bind Activin, BMP-7, and GDF-5 ligands that were immobilized onto a CM5 sensor chip was measured by SPR as previously described.[24] Briefly, the CM5 sensor chip was equilibrated with HBS-EP buffer [10 mM HEPES, 150 mM NaCl, 3 mM EDTA, and 0.005% P-20 (pH 7.4)] at a flow rate of 5 μL/min. A final surface of ∼300 RU was used to perform the flow-through assay of the receptor ECD on the Biacore 3000 with control software. The receptor ECD at various concentrations was diluted with HBS-EP buffer, injected for 6 min at a flow rate of 5 μL/min, followed by a 6 min dissociation period. The surface was regenerated with 4 M guanidine hydrochloride for 30 s at a flow rate of 10 μL/min and buffer for 30 s at a flow rate of 100 μL/min. Flow cell 1 on the CM5 chip without immobilized ligand was used as a reference. The data from flow cell 1 (activated and blocked) without immobilized ligand were referenced and subtracted using Scrubber version 2.0a BioLogic from The University of Utah. The results were plotted using Origin 7.0 (Origin Corp., Northampton, MA). All data in triplicate were analyzed with the reference subtracted.

Near- and Far-UV CD Spectroscopy and Fluorescence Determinations. CD measurements were performed on an AVIV (Lakewood, NJ) model 60DS spectropolarimeter using published procedures.[31] Fluorescence measurements were performed on a Horiba (Edison, NJ) Jobin Yvon Fluoromax-3 Fluorometer following published procedures.[32] Briefly, fluorescence spectra from 310 to 600 nm were recorded with 295 nm excitation at 25 °C. Binding constants were calculated following the Hill model using the equation $F_{obs} = F_{max}[\text{bis-ANS}]^n/(K' + [\text{bis-ANS}]^n)$, where F_{obs} and F_{max} represent the peak fluorescence intensity observed at a defined bis-ANS concentration and at a defined amount of protein, respectively, and [bis-ANS] is the concentration of the dye. The Hill coefficient n represents the number of classes of bis-ANS binding sites on the protein and is unity in the case of a single noninteractive site. A value that is greater than unity suggests positive cooperativity. K' is the apparent binding constant.

Computation Analysis. *Stability Calculation.* The connectivity of different structural elements in BMPR-II was studied by computation to provide a rationale for the functional behavior of the BMPR-II mutants. The computation was accomplished by using the COREX/BEST algorithm in a server located at the University of Texas Medical Branch (http://best.utmb.edu/BEST/), where conformational ensembles were generated for the wild-type and mutant BMPR-II ECDs. The basic approach followed that employed for the study of DHFR in our laboratory.[33] Briefly, the residue stability constant, $K_{f,j}$, is the ratio of the summed probability of all states in the ensemble in which a particular residue j is in a folded conformation ($\sum P_{f,j}$) to the summed probability of all states in which that residue is in an unfolded conformation ($\sum P_{nf,j}$):

$$\kappa_{f,j} = \frac{\sum P_{f,j}}{\sum P_{nf,j}}$$

The important feature of the residue stability constants is the fact that they provide a measure of the local stability around each residue that can be experimentally verified by comparison to hydrogen exchange protection factors. Using the high-resolution X-ray structure of BMPR-II[12] as a template, an ensemble of BMPR-II EDC conformations was generated and the residue stability constants were calculated with a modified version of COREX that employs a Monte Carlo sampling strategy. High stability constants signify residues that are folded in the majority of highly probable states under native

conditions, whereas lower stability constants signify residues that are unfolded in many of those states.

Autodock Suite. Autodock, Autogrid, and Autodock Tools were used to reproduce and predict binding sites in the complex of BMP−BMPR receptors and involved these four steps.

Step 1. Preparing Coordinate Files for the Ligand and Receptors. As control experiments to verify the ability of Autodock to capture the correct structures of BMP−BMPR receptors in the literature, we downloaded the structures from the PDB. In the case of a PDB structure that contains the ligand−receptor complex, the ligand was translated and rotated with arbitrary vectors using PyMol. Thus, the calculations were not biased to find the binding site. Then both the ligand and the receptor were saved in different PDB files. This was done for control structures. For other structures, where the ligand and receptor were in different files, it is necessary to verify that there were no clashes between the ligand and receptor structures. In case they showed clashes, translation and rotation were conducted on the ligand. To launch the calculations, the PDB files were modified to delete water molecules, hetero atoms, and added hydrogen atoms. This was accomplished by Autodock Tools (see refs 34 and 35 for details). Control calculations were conducted with the following five sets of complexes: (1) Activin receptor II−BMP-7 (PDB entry 1LX5), (2) BMP receptor IA with the Activin receptor IIB−BMP-2 dimer (PDB entry 2H62), (3) TGF-β receptor type II with TGF-β3 (PDB entry 1KTZ), (4) TGF-β receptor type I, TGF-β receptor type II, and TGF-β3 (PDB entry 2PJY), and (5) Activin receptor IIB−Activin dimer (PDB entry 1S4Y).

Step 2. Calculating atomic affinity potentials. Using the program Autogrid, precalculations of the atomic affinity potential for each atom in ligand were conducted; i.e., the receptor was embedded in a virtual box to calculate the affinity between the receptor and ligand surfaces using a probe atom.[35]

Step 3. Docking a Ligand on the Receptor. With Autodock, the final calculations and positions of the ligand on the receptor were conducted to generate a set of data based on interacting energy. This program provided a log file with coordinates and energy values for each configuration of the ligand−receptor complex. By default, the log file contained the top 10 possible conformations.

Step 4. Analyzing the Results. The log file obtained by previous steps was loaded into Autodock Tools and analyzed for geometric consistency of the ligand−receptor complex. If one of these structures were found in nature as a dimer or trimer, the calculated conformation must keep space to these other subunits. Then, according to the ranking of energy values, the best conformation was chosen as the final result.

RESULTS

Biological Activities of Mutants. The bioactivity of these receptor proteins was measured using two different assays: (A) the cell-based osteocalcin promoter activity assay and (B) the in vitro SPR studies.

A. Cell-Based Bioactivity Assay. A.1. Naturally Occurring Single-Amino Acid Substitution Mutants. Three representative naturally occurring mutants Y40X, G47N, and S107P were selected for this study. A key rationale for selecting these mutants for this study was that the mutated amino acid residues are located in two different loop regions of the BMPR-II structure with respect to the hydrophobic patch in finger 2, which has persistently been identified in other receptor−ligand complexes as part of the ligand−receptor interface (Figure 1). Furthermore, these mutations resulted in pulmonary arterial hypertension; thus, they most likely play important roles in the normal functions of BMPR-II.

The osteocalcin promoter activity assay determines the ability of the soluble BMPR-II ECD mutants to compete with the wild-type cell surface receptor for a fixed concentration of the BMP-7 ligand, resulting in a change in the available BMP-7 ligand to bind cell surface receptors. BMP-7, a BMPR-II ligand known to stimulate osteocalcin (OC) gene expression in a concentration-dependent manner in primary FRC cultures, was used as a test ligand.[24,36] Accordingly, FRC cultures were transfected with an OC promoter−Luc reporter DNA construct followed by treatment with a fixed concentration of BMP-7 (6 nM) in the absence or presence of a 20-fold molar excess of soluble wild-type or mutant BMPR-II ECD proteins. In agreement with published results, BMP-7 alone stimulated OC promoter activity by 14-fold beyond the empty plasmid control. For ease of comparison, the rest of the data obtained in the presence of the different soluble BMPR-II ECDs are expressed as relative activity with respect to that of the BMP-7 alone in the absence of any competing soluble receptor (as 1). As shown in Figure 3A, in the presence of the wild-type (WT) BMPR-II ECD, the BMP-7-stimulated OC promoter activity was reduced to ∼60% of the empty plasmid control.[a] The observation indicates that the soluble wild-type BMPR-II ECD was capable of binding BMP-7, thus reducing the "effective" BMP-7 ligand to act on the cell surface receptor and stimulating the OC−Luc reporter. In the presence of Y40Q and Y40R, the BMP-7-stimulated OC promoter activity was reduced to ∼60 and ∼70%, indicating that the ECDs of these two mutant receptors were as effective in binding BMP-7 as wild-type BMPR-II. On the other hand, in the presence of G47N, the BMP-7-stimulated OC promoter activity was not changed, indicating that the mutant was not effective in binding BMP-7 under these experimental conditions. In the presence of S107P, the BMP-7-stimulated OC promoter activity was reduced to ∼80%. These data, which are obtained by a cell-based assay, allow assessment of the relative activity of mutant receptors. Hence, the Y40Q, Y40R, and S107P mutants are effective competitors of WT BMPR-II in binding BMP-7 (6 nM) with an apparent affinity similar to that of the WT BMPR-II ECD, while the G47N mutant is not. Figure 3C shows the difference in the stimulation of the OC promoter activity in the presence of the Y40, G47, and S107 receptor mutants.

A.2. Chimeric and Deletion A-Loop Mutants. Our previously published study with various single mutations in the A-loop did not show any perturbations of binding, leading to our conclusion that the A-loop of BMPR-II did not appear to play a significant role in ligand binding.[24] However, on the basis of sequence alignment with other type II receptors of known structures but without the benefit of a holo BMPR-II structure, Mace et al.[12] suggested that five residues in the A-loop should be involved in ligand binding. Moreover, published data indicated that the A-loop in ActR-II and that of BMPR-II may play different roles in ligand binding.[11,13−16,24] The A-loop of BMPR-II extends from S86 to E98, while that of ActR-II is three residues shorter and extends from D62 to Q70 (Figure 2A). We tested the validity of the results in the literature by constructing chimeric receptor molecules in which the A-loop was swapped between ActR-IIB and BMPR-II. The chimeric receptor ABA consists of the ActR-II sequence except substituting its A-loop sequence with the BMPR-II A-loop

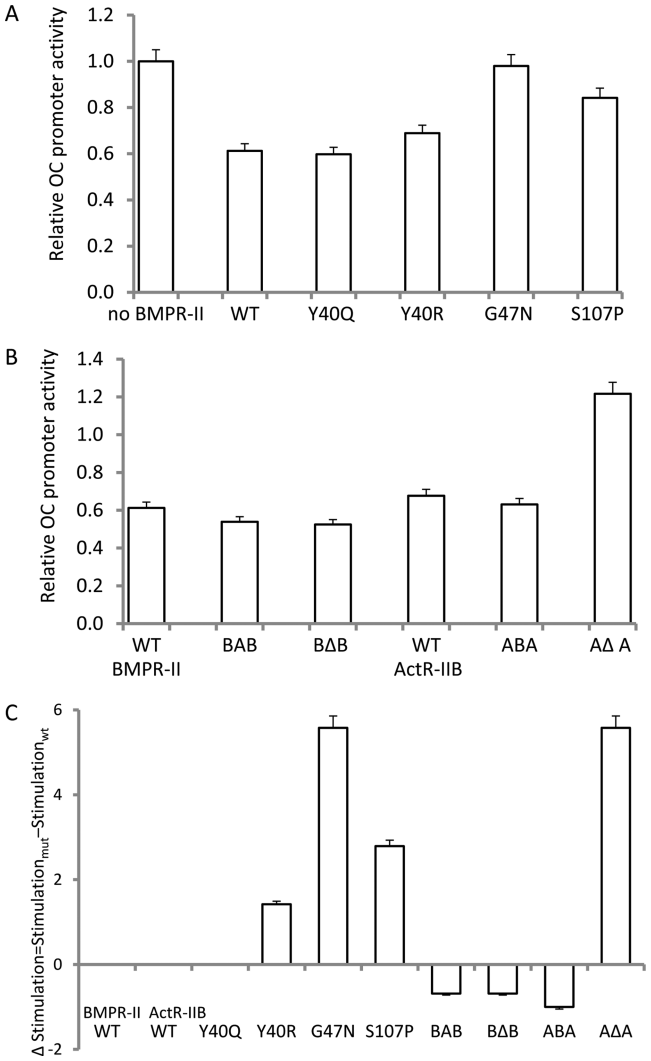

Figure 3. Osteocalcin (OC) promoter–Luc reporter activity assay. The bioactivity of the mutant ECDs of (A) BMPR-II natural mutants and (B) A-loop mutants in binding a ligand was measured by their ability to bind BMP-7 ligand and stimulate OC promoter activity in FRC cells. Confluent FRC cultures were transfected with an OC–Luc reporter plasmid. After 5 h, transfected cells were recovered in αMEM complete medium with 10% FBS overnight and then treated with 6 nM BMP-7 in the absence or presence of a 20-fold molar excess of wild-type (WT) or mutant ECDs. Luciferase reporter activity was measured as described in Materials and Methods. (C) Differences in stimulation of the OC–Luc reporter activity (Δstimulation = stimulation$_{mutant}$ − stimulation$_{wt}$) in the presence of the different mutant receptors calculated using the data shown in panels A and B. Values represent the means ± the standard error of the mean of three independent measurements.

sequence. The chimeric receptor BAB consists of the BMPR-II sequence except substituting its A-loop with the ActR-IIB A-loop (Figure 2B).

The ability of the soluble chimeric A-loop mutant receptors to bind to 6 nM BMP-7 ligand thus reducing the ligand concentration for binding cell surface receptors was tested using FRC cells.[24,36] As shown in Figure 3B, in the presence of wild-type BMPR-II, the BMP-7-stimulated OC promoter activity was reduced to 60%, indicating that soluble wild-type BMPR-II was capable of binding BMP-7, thus reducing the effective concentration of BMP-7 to act on the cell surface receptor and stimulating the OC promoter. In the presence of BAB and the BΔB BMPR-II ECD, the BMP-7-stimulated OC promoter activity also was reduced to ~55%, indicating that these two mutants were as effective in binding to 6 nM BMP-7 as the wild-type BMPR-II ECD. On the other hand, in the presence of wild-type ActR-II, the BMP-7-stimulated OC promoter activity was reduced only to ~70%, indicating that soluble ActR-II was not as effective as the WT BMPR-II ECD in binding to 6 nM BMP-7. In the presence of the soluble ABA ActR-II ECD, the BMP-7-stimulated OC promoter activity was reduced to 63%. Most interestingly, in the presence of the soluble AΔA ActR-II ECD, the BMP-7-stimulated OC promoter activity was not inhibited, suggesting that the affinity of the soluble AΔA ActR-II ECD was low and was not capable of binding to 6 nM BMP-7. Taken together, these results indicate that the BMPR-II ECD is capable of binding the BMP-7 ligand equally well with or without the A-loop, whereas in the ActR-II ECD, the presence of the A-loop from BMPR-II is essential. Without the A-loop from BMPR-II, the ActR-II ECD is not capable of binding or binds only with significantly weakened affinity for BMP-7. For ease of comparison, Figure 3C shows the difference in stimulation of the OC promoter activity in the presence of the different A-loop receptor mutants.

B. Ligand Binding Energetics of Mutants. B.1. Naturally Occurring Single-Amino Acid Substitution Mutants. SPR assays were also used to evaluate effects of the single-amino acid substitution of BMPR-II on ligand binding activity and specificity. Three ligands (Activin, BMP-7, and GDF-5) were selected for the study mainly because they are members of different BMPs subfamilies. Representative sensorgrams are included in Figure S1 of the Supporting Information. It is important to note that the sensorgrams all returned completely to the baseline after buffer injection. These results indicated the complete reversibility of receptor–ligand interactions in this study.

Panels A–C of Figure 4 show the interaction between immobilized Activin, BMP-7, and GDF-5, respectively, and varying concentrations of the wild-type and mutant receptors. The relative apparent equilibrium binding constants ($K_{d\ app}$)[b] derived from the data for each mutant receptor for Activin, BMP-7, and GDF-5 are listed in Table 1.

Effects on ligand binding affinities of single-amino acid substitutions in BMPR-II were further evaluated by calculating changes in ΔG ($\Delta\Delta G$) values, using the following equations: $\Delta G = -RT \ln(K_d)$, and $\Delta\Delta G = \Delta G_{mutant} - \Delta G_{wild\ type}$ (Figure 5A). A positive or negative value for $\Delta\Delta G$ means that the mutation weakens or enhances, respectively, the affinity versus that of the wild-type ligand. The data show that all of the substitutions of amino acid residue Y40 differentially disrupted ligand binding affinities, namely, suppression of affinity for Activin but enhancement of affinity for GDF-5 with little or no effect for BMP-7. However, substitutions at G47 and S107 enhanced the affinity for only BMP-7 and GDF-5. Thus, residues Y40, G47, and S107 all seem to play a role in differentiating various ligands. The SPR results are in general agreement with the trend of the cell-based bioactivity assay data with respect to BMP-7, i.e., suppression of affinity by Y40 mutations as compared to the other mutations.

B.2. Chimeric and Deletion A-Loop Mutants. Interactions between immobilized Activin, BMP-7, and GDF-5 ligands and varying concentrations of ActR-IIB, BMPR-II, and their respective chimeric and deletion mutants are shown in panels

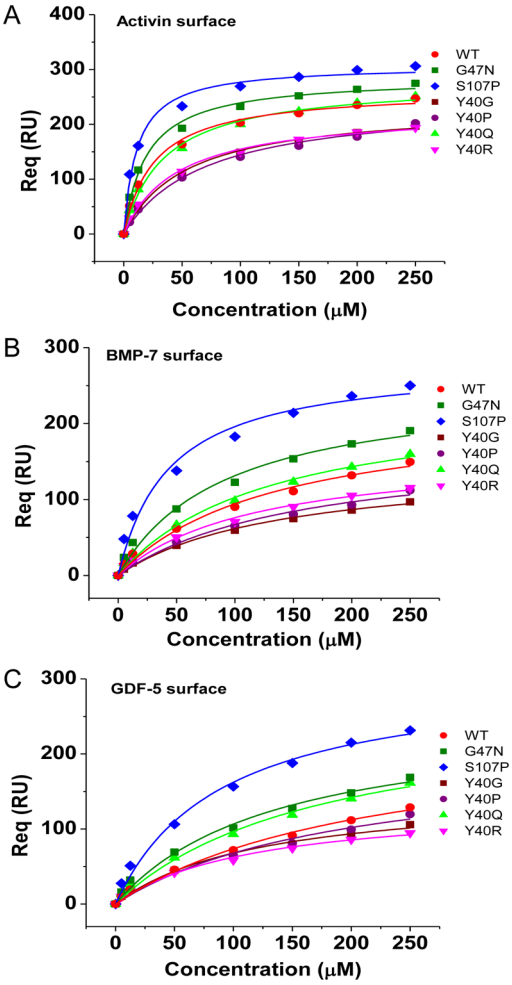

Figure 4. Ligand binding activity of wild-type and Y40G, Y40P, Y40Q, Y40R, G47N, and S107P BMPR-II mutant receptors. The bioactivity of the mutant forms of BMPR-II was determined by SPR with (A) Activin, (B) BMP-7, and (C) GDF-5 immobilized on CM-5 chips. The response at equilibrium (R_{eq}) of each sensorgram was plotted vs the concentration of each receptor protein. All data in triplicate were analyzed with the reference subtracted. The points are actual experimental data, and the curves are the results of best fits of nonlinear regression analysis of the data.

A–C of Figure 6, respectively. Representative sensorgrams are included in Figure S2 of the Supporting Information. The relative apparent equilibrium binding constants ($K_{d\ app}$) derived from the data on each receptor for these ligands are listed in Table 1. The binding results are expressed as $\Delta\Delta G$, i.e., $\Delta G_{mutant} - \Delta G_{wild\ type}$, as shown in Figure 5B. The data show that substitution of the A-loop of ActR-IIB with that from BMPR-II (ABA) led to a positive $\Delta\Delta G$ value for BMP-7; i.e., replacement with the BMPR-II A-loop suppressed its affinity for BMP-7. Surprisingly, substitution of the A-loop of BMPR-II with that from ActR-IIB (BAB) led to a negative $\Delta\Delta G$ value, i.e., increased its affinity for BMP-7. These results imply that there is a guest–host relationship between the A-loop and the rest of the receptor molecule in defining the affinity for the ligand. In other words, there is communication between the A-loop and the rest of the receptor molecule. A similar conclusion can be derived from the results for the ligand Activin, which showed essentially no affinity for the chimeric receptor ABA but an enhancement in the affinity for BAB. Activin and BMP-7

Table 1. Apparent K_d Values[a] for the Interaction of the Wild Type and BMPR-II Variants with Immobilized Activin, BMP-7, and GDF-5 As Determined by SPR

receptor	Activin (μM)	BMP-7 (μM)	GDF-5 (μM)
BMPR-II			
wild type	26 ± 1 (1.0)	135 ± 8 (1.0)	221 ± 13 (1.0)
Y40G	54 ± 2 (2.1)	138 ± 8 (1.0)	123 ± 6 (0.6)
Y40P	70 ± 4 (2.7)	157 ± 7 (1.2)	200 ± 9 (0.9)
Y40Q	35 ± 2 (1.3)	129 ± 5 (1.0)	175 ± 9 (0.8)
Y40R	46 ± 2 (1.8)	117 ± 5 (0.9)	117 ± 5 (0.5)
G47N	30 ± 2 (1.1)	92 ± 5 (0.7)	136 ± 7 (0.6)
S107P	23 ± 1 (0.9)	43 ± 2 (0.3)	90 ± 5 (0.4)
chimera BAB[b]	5 ± 1 (0.2)	59 ± 2 (0.4)	197 ± 8 (0.9)
BΔB[b]	94 ± 5 (3.6)	27 ± 1 (0.2)	BDL
ActR-IIB			
wild type	6 ± 1 (1.0)	16 ± 1 (1.0)	BDL
chimera ABA[b]	117 ± 5 (7.3)	BDL	BDL
AΔA[b]	BDL	30 ± 2 (1.9)	BDL

[a]Normalized K_d values shown in parentheses were obtained by normalization to the wild-type values. Values represent the means ± the standard error of the mean of three independent determinations with two different ligand chips and three different receptor preparations. BDL, below the detection limit (apparent K_d ~ 1300 μM). [b]BAB is the chimeric receptor consisting of BMPR-II with the ActR-IIB A-loop. BΔB is BMPR-II without its A-loop. ABA is the chimeric receptor consisting of ActR-IIB with the BMPR-II A-loop. AΔA is ActR-IIB without its A-loop.

binding was strongly affected by deletion of the A-loop of BMPR-II (BΔB) with a $\Delta\Delta G$ value that was essentially equal in magnitude but opposite in direction, i.e., suppression of affinity for Activin but enhancement for BMP-7. Another interesting observation is that the deletion of the A-loop from ActR-IIB leads to an enhancement of the affinity for the BMP-7 ligand. Because the A-loop is more dynamic, as reflected by the *B* factor in X-ray crystallographic data and the computational results shown in Figure 7, the results of binding of the BMP-7 ligand to the A-loop deletion mutants imply that BMP-7 binding is favored by a receptor that is less dynamic, but the opposite conclusion might be derived for Activin. That the level of GDF-5 binding was below the level of detection in these A-loop mutants suggests that binding of GDF-5 to these two receptors is very sensitive to the A-loop.

Structural Probing of Mutants. *Structural Integrity of Mutants. Naturally Occurring Single-Amino Acid Substitution Mutants.* The ECDs of these mutant proteins were produced in *E. coli* and purified to homogeneity using a multiple-chromatographic step procedure.[24,30] The wild-type BMPR-II proteins produced using this protocol are properly folded as analyzed by NMR[30] and are biologically active.[24] Similarly, all mutants in this study are properly folded. In this study, we used several biochemical means to examine the folding of the mutant proteins, viz., circular dichroism (CD) and fluorescence spectroscopy.

Far-UV analysis, which reveals the secondary structure of the protein, showed that all ECDs of these mutant receptors exhibited similar negative ellipticity at 205 nm corresponding to β-sheets (Figure S3 of the Supporting Information). Near-UV analysis that mostly monitors the environments surrounding aromatic amino acid residues showed that all ECDs exhibited similar positive ellipticity at 250 nm. Very minor changes were

dx.doi.org/10.1021/bi3003023 | *Biochemistry* 2012, 51, 6968–6980

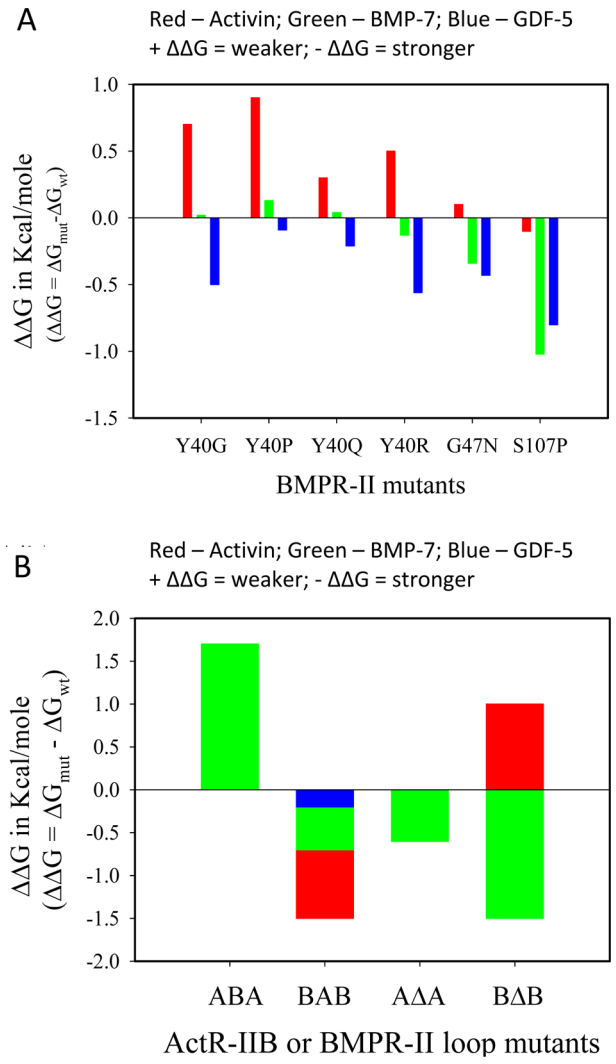

Figure 5. Changes in the binding free energy ($\Delta\Delta G$) of different BMP ligands for (A) the different natural mutants and (B) the A-loop chimera mutants. $\Delta\Delta G$ values were calculated from the equation $\Delta\Delta G = \Delta G_{mutant} - \Delta G_{wild\ type}$, where $\Delta G_{wild\ type}$ and ΔG_{mutant} are the free energies for dissociation of ligand−receptor complexes with the wild-type and mutant receptor, respectively. Values are calculated using the formula $\Delta G = -RT \ln(K_d)$. Values for Activin, BMP-7, and GDF-5 are colored red, green, and blue, respectively, for each mutant. An estimate of the upper detection limit is ~3 kcal/mol. Some of the values are close to zero and thus are not visible in the graph.

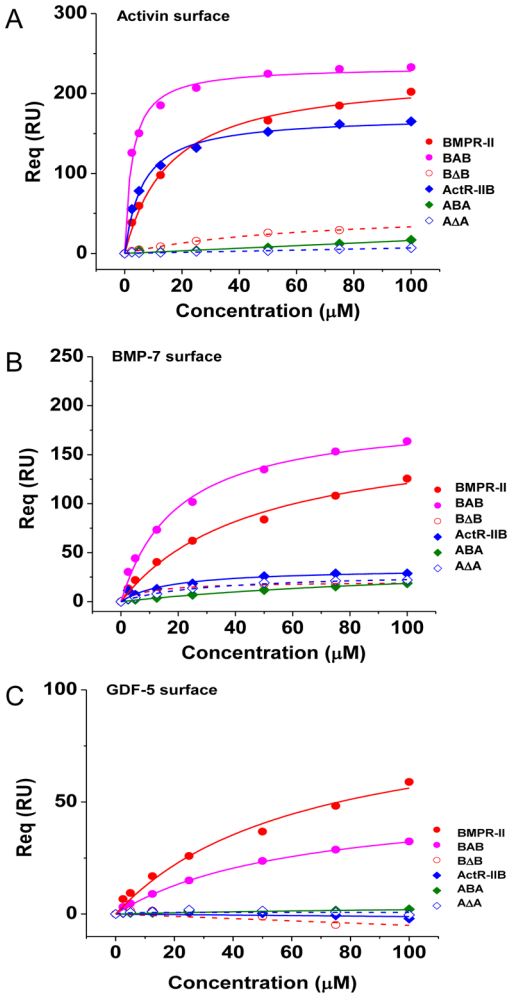

Figure 6. Bioactivity of wild-type, chimera, and A-loop-deleted ActR-IIB and BMPR-II as determined by SPR with immobilized ligands. The bioactivity of the different receptors was determined by SPR with (A) Activin, (B) BMP-7, and (C) GDF-5 immobilized on CM-5 chips. Experimental conditions were similar to those described in the legend of Figure 4.

detected in Y40G and Y40Q, and no significant structural changes were detected in the other mutants. Thus, we can conclude that the mutants are folded mainly like the wild-type protein with minor perturbations in the environment of the aromatic residues of the G and Q mutations of residue Y40.

Authors of the published X-ray crystallographic studies proposed that interactions between forms of ActR-II and BMP ligands are driven mainly by hydrophobic forces.[11,14] The proposed thermodynamic driving force is based on the fact that many of the residues that lie within the hydrophobic patch have been shown to be critical for ligand binding (Figure 1).[11,13] On the basis of these published results, we thus used bis-ANS fluorescence to examine whether any of the mutations under investigation affected the integrity of the hydrophobic patch of BMPR-II. This approach was shown previously to be able to monitor the structural integrity of the hydrophobic regions of BMPR-II.[32] Accordingly, we determined the fluorescence intensity of bis-ANS upon interaction with the wild-type and mutant receptors. The fluorescence intensity increased as a function of bis-ANS concentration with a negligible inner filter effect (data not shown). The data were further analyzed using the Hill equation and yielded K' values for bis-ANS binding (Table 2). On the basis of the K' values, the property of the bis-ANS-binding hydrophobic region appeared to be affected marginally by the different substitutions of Y40 with a maximum of 2−3-fold changes in affinity. Taken together, these results suggest that the microenvironment of the hydrophobic patch is marginally modulated by mutations. If the hydrophobic patch in BMPR-II is indeed involved as the interface for ligand interaction, then the binding of ligands is expected to be modulated by mutations that seem to perturb the microenvironment of the hydrophobic patch.

Additionally, we used fluorescence energy transfer (FRET) to examine the structural integrity of the BMPR-II mutant ECD. Previously, we showed the presence of one bis-ANS binding site per BMPR-II ECD protein molecule.[32] In this study, we observed FRET as evident from the overlap of the tryptophan fluorescence emission spectrum of all the forms of

dx.doi.org/10.1021/bi3003023 | *Biochemistry* 2012, 51, 6968−6980

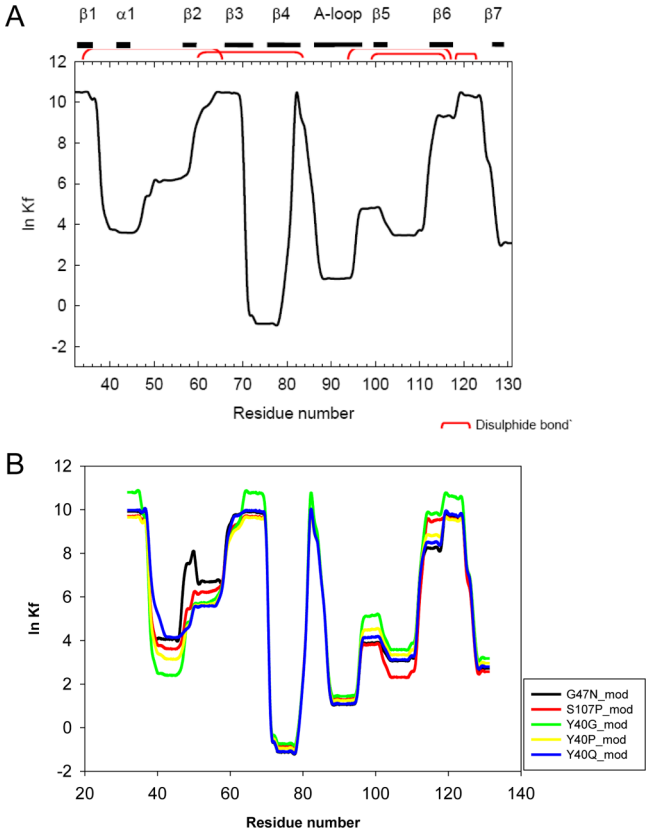

Figure 7. Computational analysis of the stability of human recombinant BMPR-II (A) wild type and (B) Y40G, Y40P, Y40Q, G47N, and S107P mutants. Calculated residue stability constants (ln K_f) for the different BMPR-II molecules are on the *Y*-axis as a function of residue number (*X*-axis). The locations of secondary structural elements and the locations of the disulfide bonds are also indicated.

Table 2. K_d Values[a] of Bis-ANS for BMPR-II

receptor	K'^b (μM)	K'^c (μM)	I_{Max} (arbitrary units)
BMPR-II			
wild type	19 ± 3 (1.0)	19 ± 3 (1.0)	6×10^4 (1.0)
Y40G	6 ± 1 (0.3)	10 ± 1 (0.6)	6×10^4 (1.1)
Y40P	34 ± 4 (1.8)	30 ± 5 (1.6)	6×10^4 (1.1)
Y40Q	45 ± 10 (2.4)	36 ± 7 (1.9)	8×10^4 (1.4)
Y40R	21 ± 2 (1.1)	17 ± 2 (0.9)	5×10^4 (0.8)
G47N	55 ± 13 (2.9)	44 ± 8 (2.3)	9×10^4 (1.7)
S107P	19 ± 3 (1.0)	17 ± 5 (0.9)	4×10^4 (0.8)
BMPR-II			
wild type	10 ± 2 (1.0)	12 ± 2 (1.0)	9×10^4 (1.0)
chimera (BAB)[d]	6 ± 1 (0.5)	6 ± 1 (0.5)	8×10^4 (0.9)
BΔB[d]	1 ± 0 (0.1)	2 ± 0 (0.1)	10×10^4 (1.1)
ActR-IIB			
wild type	3 ± 1 (1.0)	3 ± 1 (1.0)	2×10^4 (1.0)
chimera (ABA)[d]	7 ± 1 (2.0)	13 ± 1 (3.8)	6×10^4 (3.0)
AΔA[d]	4 ± 1 (1.2)	5 ± 1 (1.4)	5×10^4 (2.5)

[a]Relative values shown in parentheses were calculated by normalization to the wild-type values. [b]Calculated according to the Hill equation: $F_{obs} = F_{max}[\text{bis-ANS}]^n/(K' + [\text{bis-ANS}]^n)$. [c]Calculated from the transfer of energy from tryptophan in BMPR-II to bis-ANS data. [d]Same abbreviations as in Table 1.

the BMPR-II ECD (wild-type and mutants) and the excitation spectrum of bis-ANS. The structural integrity of W85 and W87 in BMPR-II might be important, because they have been postulated by Mace et al.[12] to interact with ligand. This observation is consistent with published results indicating the proximity of the tryptophan residues and the bis-ANS binding site.[32] The observed transfer of energy between bis-ANS and tryptophan is consistent with assigning the hydrophobic residues in finger 2 as the primary site for bis-ANS binding. The two tryptophan residues reside at the edge of the hydrophobic patch located in the β-sheets that constitute finger 2. The K' values calculated by energy transfer are listed in Table 2. The K' values determined by the titration method and FRET were in agreement. The findings also suggested that all mutant ECDs exhibited similar, if not identical, folding regarding the bis-ANS reactive hydrophobic region and the tryptophan residues.

Chimeric and Deletion A-Loop Mutants. The folding of these chimeric receptors was studied using the same fluorescence approaches, namely, the binding of bis-ANS and FRET. Analysis of the bis-ANS binding data using the Hill equation yielded K' values as summarized in Table 2. The results suggest that the A-loop of BMPR-II can be replaced by that of ActR-II but with significant perturbation of the accessibility of the bis-ANS-binding hydrophobic region. Deletion of the A-loop from BMPR-II also altered the microenvironment of the hydrophobic region. The A-loop of ActR-IIB also can be replaced by that of BMPR-II but with significant perturbation of the microenvironment of the ActR-IIB molecule. In contrast to BMPR-II, deletion of the A-loop of ActR-IIB did not appear to perturb this region significantly.

In the FRET experiments, we observed the transfer of fluorescence energy from the overlap of the tryptophan fluorescence emission spectrum of the wild-type BMPR-II ECD as well as the chimera receptors and the excitation spectrum of bis-ANS. The K' values calculated by energy transfer are listed in Table 2. The apparent dissociation constants determined by the fluorescence titration method and FRET for all chimeric receptors, except the ABA chimera, were consistent with each other. For the ABA chimera, the K' value determined by FRET is almost twice that determined by fluorescence titration, suggesting that the folding of the ABA molecule differed from that of the wild type, and the spatial relationship between the tryptophan residues and the bis-ANS binding site was altered. However, folding of the AΔA mutant did not appear to be perturbed. The BAB chimera reacted with bis-ANS with a smaller K' value, suggesting that the hydrophobic regions of the chimeric receptor are more exposed. Deletion of the A-loop from BMPR-II resulted in a dramatic exposure of hydrophobic regions, suggesting that the A-loop of BMPR-II is an important structural determinant.

Structural Stability of Mutants. The ensemble-based COREX/BEST algorithm[33] was used to evaluate effects of the mutation on the protein stability of BMPR-II (Figure 7A,B). The analysis expresses the stability (*Y*-axis) of each residue in BMPR-II (*X*-axis); amino acid residues with lower ln k_f values indicate low stability. Figure 7A shows the results for wild-type BMPR-II. Regions around residues 40−46, 70−80, and 88−96 are less stable than regions around residues 66−70. The three amino acid residues of interest (Y40, G47, and S107) are located in two different low-stability regions. It is interesting to note that residues L69, I77, L79, V80, I88, V100, V101, and I108 in the hydrophobic patch in finger 2 reside mostly in low-

dx.doi.org/10.1021/bi3003023 | *Biochemistry* 2012, 51, 6968−6980

Table 3. Contact Residues[a] in the BMPR-II ECD between Ligand Activin, BMP-7, or GDF-5 and BMPR-II Predicted by Autodock

ligand−receptor	complex	finger 1	finger 2	finger 3	A-loop
Activin−BMPR-II	I	**Y40**, D43	L69	P106, Y113	**W85**, S86, D90
		L44, **I46**			P91, Q92
	II	**I46**	K81	P106, Q109	**W85**, Q92
BMP-7−BMPR-II	I	**Y40**	Y67, K81	P105, P106, Q109	**W85**, D90, P91
			C84	N110, Y113, F115	
	II	L44, **I46**		P105, P106, Q109	**W85**, S86, H87
					D90, P91, Q92
GDF-5−BMPR-II	I		C84	P105, P106, I108	**W85**, H87
				Q109	D90, P91, Q92
	II	D38, **Y40**	Y67, L69, E71	Y113	**W85**, H87, I88
		I46	V80, K81, C84		G89, D90, P91

[a]Residues in bold denote the residues common to all three predicted receptor−ligand complexes.

stability regions. Actually, residues 40−46, 71−76, and 102−112 constitute the tips of fingers 1−3, respectively. In addition, the A-loop that consists of residues 89−98 is also shown to be less stable. The computation analysis suggests that these regions are dynamic, a conclusion consistent with the distribution of *B* factors in the X-ray structure.[12] Thus, the results derived from the COREX/BEST algorithm can capture the essence of dynamics of the structure defined by high-resolution techniques such as X-ray crystallography.

Figure 7B shows the effects of mutations on the stability profiles of the BMPR-II ECD. The general stability profile of these mutants has not changed significantly, although the specific value of ln k_f has changed, particularly that of Y40G. The most interesting and significant observation is that the perturbation of stability not only occurs at the mutation site but also is propagated to other parts of the molecule; i.e., there is long-range communication among these sites. For example, the stability of regions consisting of residues 65−70 and 95−125 is affected by the Y40G mutation. However, residue Y40 is located in finger 1, whereas residues 65−70 and 95−125 are in fingers 2 and 3, respectively.

Computational Docking of Ligands to the BMPR-II ECD. To further elucidate the understanding of the results of our functional and solution structural studies at the molecular level, we conducted a computational docking exercise. In the control set of calculations, we used the following five complexes with known structures at the atomic level: (1) Activin receptor II−BMP-7 (PDB entry 1LX5), (2). BMP receptor IA with Activin receptor IIB−BMP-2 dimer (PDB entry 2H62), (3) TGF-β receptor type II−TGF-β3 (PDB entry 1KTZ), (4) TGF-β receptor type I with TGF-β receptor type II−TGF-β3 (PDB entry 2PJY), and (5) Activin receptor IIB−Activin dimer (PDB entry 1S4Y). In all cases, the computational results yielded a structure of the complex with a root-mean-square deviation of <0.1 Å in reference to their crystal structures. Thus, we have been successful in capturing the atomic structures of the complexes with a 1:1 stoichiometry, but it was difficult to obtain unique solutions with the dimeric ligands because the computation resulted in more than one structure for the ligand−receptor complex with very similar energetics. Because the systems under investigation are 1:1 complexes, we proceeded to explore the molecular structures of complexes of the BMPR-II ECD with Activin, BMP-7, and GDF-5 as ligands. The emphasis was on the general interfacial contacts within a radius of 4 Å between the residues in the receptor and ligands. Results of this exercise are summarized in Table 3. In all cases, there are two structures of equal probability as gauged by the energetic of complex formation. In Figure 1, the structure of the BMPR-II ECD is shown to highlight the three fingers and A-loop. The contacts of the two most probable Activin−BMPR-II complexes are listed in Table 3. The interfacial interactions in the first probable complex involved BMPR-II residues D43, L44, and I46 in finger 1, residue L69 of the hydrophobic core of finger 2, and residues P106 and Y113 at the tip of finger 3. The Activin−BMPR-II alternative complex involved contacts with I46 in finger 1, K81 in finger 2, P106 and Q109 in finger 3, and the A-loop of the receptor. The interfacial contacts in the BMP-7−BMPR-II probable complexes involved finger 3 and the A-loop of the receptor, but the alternative probable BMP-7−BMPR-II complex inferred that contacts involve fingers 1 and 3 and residues in the A-loop of the receptor (Table 3). The interesting exception was the lack of probable contacts with finger 2 of the receptor. The contacts of the two GDF-5−BMPR-II probable complexes are shown in Table 3. In one probable complex, no contacts were probable with finger 1, although contacts were probable with residues in fingers 2 and 3 and the A-loop of the receptor. In the GDF-5−BMPR-II alternative complex, the pattern was different with probable contacts with all fingers and the A-loop of the receptor.

Another interesting result derived from this computation exercise is that residues Y40 and I46 in finger 1 and W85 in the A-loop of the receptor were identified to be the common residues in contact with all three ligands. Consistent with the computational results are data of others and our experimental data showing the effects of mutation of Y40 on the ability of BMPR-II to distinguish among ligands Activin, BMP-7, and GDF-5. We and others previously also demonstrated the effect of mutating W85 on the affinity of binding to BMP-2, BMP-7, and GDF-5.[8,24]

Figure 8 summarizes the results of this docking exercise. The three residues in fingers 1 and 2 of the receptor that make contact with all three ligands are shown as spheres, while the other residues in contact with at least one ligand are shown as dots. It is interesting to note that all three fingers have residues that make contacts with ligands, and they all reside on one face, the concave side, of BMPR-II.

DISCUSSION

In this study, we aimed to elucidate the molecular mechanism used by the two type II BMP receptors in defining specificity and/or affinity in ligand binding. Although the ECD of BMPR-

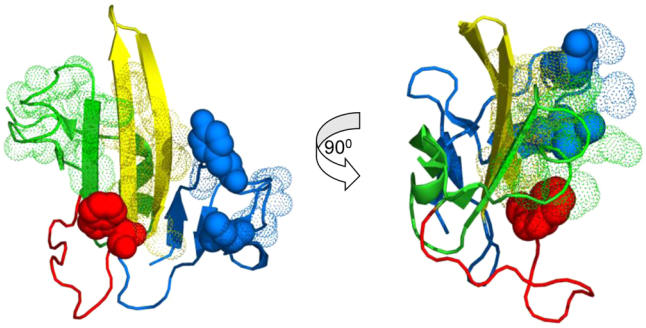

Figure 8. Summary of important residues involved in interfacial interaction between BMPR-II and ligands. The three residues in fingers 1 and 2 that make contact with all three ligands are shown as spheres, while the other residues in contact with at least one ligand are shown as dots. The color codes for the residues are as follows: blue spheres for residues Y40 and I46 and red sphere for W85.

II has a sequence only 24% identical to that of its closely related ActR-IIB (Figure 2A), they have essentially identical folding (Figure 1). One may expect these ECDs to have similar functional and structural behaviors. In this study, we tested the validity of this assumption.

Effects of Natural Mutations. This study focused on two different structural elements, namely, fingers 1 and 3. Specifically, mutants involving residues Y40, G47, and S107 were studied because previously they were detected in patients suffering from pulmonary arterial hypertension. These amino acids are not among the residues predicted to be part of the binding interface as a consequence of analogy analysis with other known structures of ligand−receptor complexes or sequence alignment. Residues in ActR-IIB that are in contact with BMP-7 are shown in Figure 1[11] and do not include Y40, G47, and P107.

If indeed these residues in BMPR-II were not in contact with the ligands but mutations of these residues affect ligand binding as shown in this study, then one interpretation is that the effect of perturbations resulted from the mutation must be the consequence of a long-range communication from these residues to the binding interface, which involves at least the hydrophobic patch identified in most ligand−receptor complexes. The current consensus in the literature is that intramolecular long-range communication is likely because proteins exist as an ensemble of microstates in dynamic equilibrium. We hypothesize that BMPR-II most likely can be represented by such an ensemble of dynamic states. The validity of this hypothesis is supported by the ability of the COREX/BEST algorithm to capture the dynamic nature of the BMPR-II structure that is defined by the atomic structure of the receptor determined by high-resolution X-ray crystallography, as shown in Figure 7. Namely, the strong dynamic nature of the finger tips and the A-loop is highly coincident with the structural elements showing low ln k values (low stability) in the computational results. The computational results are consistent with experimental data such as high B factor in the X-ray data.[24] Thus, COREX/BEST is capable of capturing the essence of BMPR-II as a dynamic entity.

A direct corollary to a dynamic entity is that each molecule exists simultaneously in multiple microstates, the distribution of which is governed by equilibrium processes that can be modulated by environmental factors such as pH, temperature, ligand binding, or mutation. Results from this study provide the expected data. For example, as observed in Figure 7, the effect of mutation of Y40 is not localized to the tip of finger 1 but also tips of fingers 2 and 3. The regions, whose stability is predicted to be the most perturbed, include residues 40−50, 60−70, and 95−125. Furthermore, the more stable regions around residues 65, 100, and 120 are further stabilized by the Y40 mutation. This analysis also shows that the expected binding interface in BMPR-II, assuming BMPR-II and ActR-IIB use the same surface area for ligand binding, includes approximately residues 60−80, 85, and 91−96 and several residues at the C-terminus. Thus, the stability of the predicted residues is affected by the mutation, and these residues are within the predicted regions of the ligand binding interface. In addition, different amino acid side chain substitutions at Y40 lead to different magnitudes of perturbations of different parts of BMPR-II. The magnitude of perturbation decreases in the following order: G > P > Q. It is gratifying to note that the binding affinity of bis-ANS for the hydrophobic patch is affected by mutations at Y40, and the magnitude of the change seems to be dependent on the nature of the substituted side chain. Thus, it is not surprising that different mutations of Y40 alone can lead to a diverse set of functional perturbations, e.g., enhancing the affinity for GDF-5 but suppressing that of Activin. Hence, in this study, the computational results of the COREX/BEST algorithm apparently can capture the essence of the functional perturbation as a consequence of mutation. This observation is consistent with the fact that the COREX/BEST algorithm has been employed successfully to capture many phenomena that require long-range intramolecular communications.[33,37−40]

The current consensus opinion in the literature is that a hydrophobic patch in the two type II receptors ActR-IIB and BMPR-II is involved in ligand binding. The location of this patch resides in Finger 2 (Figure 1). Based on crystallographic data of the apo BMPR-II, Mace et al. proposed that Y67, W85, and F115 as the residues in the hydrophobic patch that are in contact with ligands.[12] They further proposed that K81, S86, E93, and Y113 are also involved. It is interesting to note that the stability of residue 67 and 115 is significantly perturbed by a Y40G mutation. This significant change in stability is correlated to the most significant changes in the binding affinity of ligands BMP-7 and GDF-5 in opposite directions as shown in Figure 5A. Furthermore, the same Y40G mutation leads to the largest change in the binding affinity for bis-ANS (Table 2). Thus, there is an apparent correlation among perturbation of residue stability, environmental integrity of the hydrophobic patch and ligand binding affinity.

On the other hand, our experimental data showed that a G47N mutation impacts on ligand binding by lowering the affinity for all ligands, though to different extents depending on the identity of the ligand. In Figure 7B the COREX/BEST computational results showed minor perturbation of the stability of a smaller number of residues in BMPR-II. The same correlation between functional and structural stability can be drawn with the S107P mutation. Thus, our results seem to indicate that Y40, G47, and S107 play different roles to differentiate ligands, and alterations of these residues are detrimental to ligand binding.

Another very interesting observation is that the affected regions seem to be anchored by the five disulfide bonds in the ECD of BMPR-II; most of them seem to be strategically located in junctions between a stable and a highly dynamic structural element. This finding implies that one function of the

disulfide bonds might be to transmit the signal to specific regions of the BMPR-II molecule and to serve a structural role.

Structural Relationship between the A-Loop and the Hydrophobic Patch. Although both BMPR-II and ActR-IIB contain an A-loop structure, results from previously published studies from different laboratories are incongruent with respect to the role of the A-loop in binding of BMPs.[11,13−16,24] These results of functional and computational studies showing a guest−host relationship between the ECD and A-loop suggest the presence of intramolecular long-range communication. Such communication can provide a rationale for the discrepancies reported in the literature.

The A loop in the BMPR-II is two amino acid residues longer than that in ActR-IIB. This study shows that deletion of the A-loop from the ActR-IIB receptor (AΔA) did not appear to affect its global fold, but substitution of the ActR-IIB A-loop with the BMPR-II A-loop (ABA) resulted in a significant alteration in the accessibility of the hydrophobic site by bis-ANS. According to the structural model, the distance between the A-loop and the hydrophobic patch is fairly substantial; thus, the change in the bis-ANS binding site must be attributed to a long-range communication between these two structural elements within the receptor. Furthermore, the observed perturbations in the hydrophobic patch are important because this region has been shown to be part of the binding interface in other ligand−receptor complexes. The finding of this study showing that the binding of ligands is affected is thus consistent. Thus, results obtained from mutation of a single amino acid residue and from A-loop substitution and/or deletion lead to the same correlation between the structural integrity of the hydrophobic patch and ligand binding.

Function of the A-Loop. Our results for the ActR-IIB and BMPR-II chimera indicate that the A-loop in the two ECD proteins plays complex and distinct functional roles. Specifically, our observations suggest that BMPR-II is more tolerant and is not that sensitive to the nature of the A-loop or its presence. As shown in Table 1, wild-type BMPR-II, the BΔB deletion mutant receptor, and the chimeric BAB receptor can all bind ligands. The data further suggest that both the BMPR-II and the BMP-7 ligand are quite promiscuous in their binding behavior. Specifically, deletion of the A-loop essentially eliminated the ability to bind ligands Activin and GDF-5 but enhanced the affinity for ligand BMP-7. Replacement of the A-loop with the shorter loop from ActR-IIB renders the chimeric receptor a better Activin binder. The observation suggests that the A-loop is dynamic, a less dynamic A-loop is better for Activin binding, and the change in the dynamic nature of the A-loop is not important for BMP-7 binding. However, computational docking analysis of the BMP-7−BMPR-II complex shows a great deal of contact between the receptor and the ligand; thus, one might expect a decrease in ligand binding affinity because of the decrease in the level of contact as a result of the shorter A-loop from ActR-IIB, yet the binding data for the chimeric receptor showed that it binds stronger. One plausible explanation of these findings is that the A-loop in BMPR-II is very dynamic and thus does not affect BMP-7 binding affinity. Consistent with this supposition are the results of published results indicating that mutations of several residues (viz., S86, H87, D90, and Q92) within the A-loop did not affect binding of BMP-2, BMP-7, or GDF-5 significantly.[24] On the contrary, mutations of L61 and D63 (which correspond to S86 and H87 in BMPR-II, respectively) in the A-loop of ActR-IIB significantly disrupted BMP-2 and BMP-7 binding.[14] Studies of the crystal structure of the BMP-7−ActR-IIB complex also revealed that several residues (L61, D63, I64, and N65) in the A-loop region of ActR-II interact with the BMP-7 ligand.[22] These findings suggest that the A-loop in the two related receptors might play a distinct role.

By comparison, ActR-IIB is not tolerant at all. Only wild-type ActR-IIB can bind both Activin and BMP-7. A replacement of the A-loop of ActR-IIB with that of BMPR-II (ABA) eliminated its ability to bind ligand Activin but still showed a demonstrable affinity for ligand BMP-7. A deletion of the A-loop renders ActR-IIB (AΔA) totally inactive toward ligands Activin and GDF-5 but creates a strong affinity for ligand BMP-7.

Results for the chimeric receptors reveal two novel observations; namely, the role of the A-loop of the receptor is dependent on the three-finger fold of the host receptor, and both BMPR-II and BMP-7 have a less stringent requirement for binding. In the context of ActR-IIB, the A-loop is critical for Activin and GDF-5 binding but contributes to BMP-7 binding.

Summary. In summary, this study has identified regions of the BMPR-II molecule that define ligand specificity. The different regions play different roles in ligand binding. An integration of these results on functional energetics and protein structures identifies, for the first time, an intradomain communication network within the BMPR-II molecule. Identification of such a communication network is important not only for understanding the working of the receptor but also for protein engineering and drug design. Furthermore, we are currently investigating one of the more intriguing and fundamental issues about the mechanism and structural entity that define promiscuity and specificity of both the ligand and receptor. Is the information imbedded in the folds? Can the three-finger fold be responsible for promiscuity? What is the mechanism that allows amino acids to exert a dominant effect on the A-loop? What is the role of the disulfide bonds in the natural mutants? These are the issues that we are actively pursuing.

■ ASSOCIATED CONTENT

Supporting Information

SPR sensorgrams and CD spectra of BMPR-II and its variants. This material is available free of charge via the Internet at http://pubs.acs.org.

■ AUTHOR INFORMATION

Corresponding Author

*Department of Biochemistry, University of Texas Health Science Center at San Antonio, 7703 Floyd Curl Dr., San Antonio, TX 78229-3900. Phone: (210) 567-3777. Fax: (210) 567-6595. E-mail: leej@uthscsa.edu.

Funding

Financial support to J. Ching Lee from the National Institutes of Health (NIH) (GM 77551) and the Robert A. Welch Foundation and to John C. Lee from NIH (AG 037746) is acknowledged.

Notes

The authors declare no competing financial interest.

■ ACKNOWLEDGMENTS

We gratefully acknowledge the technical assistance of Yao Xiao. For the SPR studies, we acknowledge the support of the University of Texas Health Science Center at San Antonio (UTHSCSA) Center for Macromolecular Interactions, which is

supported in part by the Cancer Therapy and Research Center through the National Institutes of Health, National Cancer Institute P30 Award CA054174, and Texas State funds provided through the Office of the Vice President for Research of the UTHSCSA.

■ ABBREVIATIONS

BMP, bone morphorgenetic protein; BMPR-II, BMP receptor-II; bis-ANS, 4,4′-dianilino-1,1′-bisnaphthyl-5,5′-disulfonic acid; SPR, surface plasmon resonance; PDB, Protein Data Bank.

■ ADDITIONAL NOTES

[a]Although inhibition of the BMP-7-stimulated OC promoter activity was observed, the inhibition was incomplete even at the highest tested receptor:ligand molar ratio of 20:1, presumably because of the relatively low affinity of the receptor for the ligand.

[b]The term apparent equilibrium binding constant is used to reflect the fact that the value is valid for a specific concentration of immobilized ligand. One does not have stringent control of the specific amount of ligand immobilized; thus, in duplicate runs with different chips of the same type of surface, different "apparent equilibrium binding constants" are observed. However, a comparison of the parameter $\Delta\Delta G$ is valid and accurate because within the same chip all the uncontrollable parameters are experienced by all the ECDs. We prefer not to complicate the process of data analysis by adding more fitting parameters such as surface activity. Additional parameters in fitting the data may obscure the actual message imbedded in the data. That is the reason we chose to express our data as $\Delta\Delta G'$.

■ REFERENCES

(1) Kingsley, D. M. (1994) The TGF-β superfamily: New members, new receptors, and new genetic tests of function in different organisms. *Genes Dev. 8*, 133−146.

(2) Reddi, A. H. (2000) Bone morphogenetic proteins and skeletal development: The kidney-bone connection. *Pediatr. Nephrol. (Berlin) 14*, 598−601.

(3) Wozney, J. M., and Rosen, V. (1998) Bone morphogenetic protein and bone morphogenetic protein gene family in bone formation and repair. *Clin. Orthop. Relat. Res. 346*, 26−37.

(4) Chen, D., Zhao, M., and Mundy, G. R. (2004) Bone morphogenetic proteins. *Growth Factors 22*, 233−241.

(5) Wagner, D. O., Sieber, C., Bhushan, R., Borgermann, J. H., Graf, D., and Knaus, P. (2010) BMPs: From bone to body morphogentic proteins. *Sci. Signaling 3*, 1−6.

(6) Reddi, A. H. (2005) BMPs: From bone morphogenetic proteins to body morphogenetic proteins. *Cytokine Growth Factor Rev. 16*, 249−250.

(7) Massague, J. (1998) TGF-β signal transduction. *Annu. Rev. Biochem. 67*, 753−791.

(8) Kawabata, M., Imamura, T., and Miyazono, K. (1998) Signal transduction by bone morphogenetic proteins. *Cytokine Growth Factor Rev. 9*, 49−61.

(9) Miyazono, K., Kusanagi, K., and Inoue, H. (2001) Divergence and convergence of TGF-β/BMP signaling. *J. Cell. Physiol. 187*, 265−276.

(10) Sebald, W., Nickel, J., Zhang, J. L., and Mueller, T. D. (2004) Molecular recognition in bone morphogenetic protein/receptor interaction. *Biol. Chem. 385*, 697−710.

(11) Greenwald, J., Groppe, J., Gray, P., Wiater, E., Kwiatkowski, W., Vale, W., and Choe, S. (2003) The BMP7/ActRII extracellular domain complex provides new insights into the cooperative nature of receptor assembly. *Mol. Cell 11*, 605−617.

(12) Mace, P. D., Cutfield, J. F., and Cutfield, S. M. (2006) High resolution structures of the bone morphogenetic protein type II receptor in two crystal forms: Implications for ligand binding. *Biochem. Biophys. Res. Commun. 351*, 831−838.

(13) Thompson, T. B., Woodruff, T. K., and Jardetzky, T. S. (2003) Structures of an ActRIIB:activin A complex reveal a novel binding mode for TGF-β ligand:receptor interactions. *EMBO J. 22*, 1555−1566.

(14) Weber, D., Kotzsch, A., Nickel, J., Harth, S., Seher, A., Mueller, U., Sebald, W., and Mueller, T. D. (2007) A silent H-bond can be mutationally activated for high-affinity interaction of BMP-2 and activin type IIB receptor. *BMC Struct. Biol. 7*, 6.

(15) Kirsch, T., Nickel, J., and Sebald, W. (2000) BMP-2 antagonists emerge from alterations in the low-affinity binding epitope for receptor BMPR-II. *EMBO J. 19*, 3314−3324.

(16) Greenwald, J., Vega, M. E., Allendorph, G. P., Fischer, W. H., Vale, W., and Choe, S. (2004) A flexible activin explains the membrane-dependent cooperative assembly of TGF-β family receptors. *Mol. Cell 15*, 485−489.

(17) Hart, P. J., Deep, S., Taylor, A. B., Shu, Z., Hinck, C. S., and Hinck, A. P. (2002) Crystal structure of the human TβR2 ectodomain-TGF-β3 complex. *Nat. Struct. Biol. 9*, 203−208.

(18) Allendorph, G. P., Vale, W. W., and Choe, S. (2006) Structure of the ternary signaling complex of a TGF-β superfamily member. *Proc. Natl. Acad. Sci. U.S.A. 103*, 7643−7648.

(19) Kirsch, T., Sebald, W., and Dreyer, M. K. (2000) Crystal structure of the BMP-2-BMPR-IA ectodomain complex. *Nat. Struct. Biol. 7*, 492−496.

(20) Kotzsch, A., Nickel, J., Seher, A., Heinecke, K., van Geersdaele, L., Herrmann, T., Sebald, W., and Mueller, T. D. (2008) Structure analysis of bone morphogenetic protein-2 type I receptor complexes reveals a mechanism of receptor inactivation in juvenile polyposis syndrome. *J. Biol. Chem. 283*, 5876−5887.

(21) Keller, S., Nickel, J., Zhang, J. L., Sebald, W., and Mueller, T. D. (2004) Molecular recognition of BMP-2 and BMP receptor IA. *Nat. Struct. Mol. Biol. 11*, 481−488.

(22) Greenwald, J., Fischer, W. H., Vale, W. W., and Choe, S. (1999) Three-finger toxin fold for the extracellular ligand-binding domain of the type II activin receptor serine kinase. *Nat. Struct. Biol. 6*, 18−22.

(23) Boesen, C. C., Radaev, S., Motyka, S. A., Patamawenu, A., and Sun, P. D. (2002) The 1.1 Å crystal structure of human TGF-β type II receptor ligand binding domain. *Structure 10*, 913−919.

(24) Yin, H., Yeh, L. C., Hinck, A. P., and Lee, J. C. (2008) Characterization of ligand binding properties of the human BMP type II receptor extracellular domain. *J. Mol. Biol. 378*, 191−203.

(25) Machado, R. D., Aldred, M. A., James, V., Harrison, R. E., Patel, B., Schwalbe, E. C., Gruenig, E., Janssen, B., Koehler, R., Seeger, W., Eickelberg, O., Olschewski, H., Elliott, C. G., Glissmeyer, E., Carlquist, J., Kim, M., Torbicki, A., Fijalkowska, A., Szewczyk, G., Parma, J., Abramowicz, M. J., Galie, N., Morisaki, H., Kyotani, S., Nakanishi, N., Morisaki, T., Humbert, M., Simonneau, G., Sitbon, O., Soubrier, F., Coulet, F., Morrell, N. W., and Trembath, R. C. (2006) Mutations of the TGF-β type II receptor BMPR2 in pulmonary arterial hypertension. *Hum. Mutat. 27*, 121−132.

(26) Roberts, K. E., McElroy, J. J., Wong, W. P. K., Yen, E., Widlitz, A., Barst, R. J., Knowles, J. A., and Morse, J. H. (2004) BMPR2 mutations in pulmonary arterial hypertension with congenital heart disease. *Eur. Respir. J. 24*, 371−374.

(27) Morrell, N. W., Adnot, S., Archer, S. L., Dupuis, J., Jones, P. L., Maclean, M. R., McMurtry, I. F., Stenmark, K. R., Thistlethwaite, P. A., Weissmann, N., Yuan, J. X. J., and Weirqq, E. K. (2009) Cellular and molecular basis of pulmonary arterial hypertension. *J. Am. Coll. Cardiol. 54*, S20−S31.

(28) Nasim, M. T., Ghouri, A., Patel, B., James, V., Rudarakanchana, N., Morrell, N. W., and Trembath, R. C. (2008) Stoichiometric imbalance in the receptor complex contributes to dysfunctional BMPR-II mediated signalling in pulmonary arterial hypertension. *Hum. Mol. Genet. 17*, 1683−1694.

(29) Sztrymf, B., Coulet, F., Girerd, B., Yaici, A., Jais, X., Sitbon, O., Montani, D., Souza, R., Simonneau, G., Soubrier, F., and Humbert, M. (2008) Clinical outcomes of pulmonary arterial hypertension in carriers of BMPR2 mutation. *Am. J. Respir. Crit. Care Med. 177*, 1377−1383.
(30) Yin, H., Ilangovan, U., Hinck, A. P., and Lee, J. C. (2005) Sequential resonance assignment of the human BMP type II receptor extracellular domain. *J. Biomol. NMR 32*, 336.
(31) Yu, S., Wuu, A., Basu, R., Holbrook, M. R., Barrett, A. D., and Lee, J. C. (2004) Solution structure and structural dynamics of envelope protein domain III of mosquito- and tick-borne flaviviruses. *Biochemistry 43*, 9168−9176.
(32) Yin, H., Zhou, Q., Panda, M., Yeh, L. C., Zavala, M. C., and Lee, J. C. (2007) A fluorescence study of type I and type II receptors of bone morphogenetic proteins with bis-ANS (4,4′-dianilino-1,1′-bisnaphthyl-5,5′-disulfonic acid). *Biochim. Biophys. Acta 1774*, 493−501.
(33) Pan, H., Lee, J. C., and Hilser, V. J. (2000) Binding sites in *Escherichia coli* dihydrofolate reductase communicate by modulating the conformational ensemble. *Proc. Natl. Acad. Sci. U.S.A. 97*, 12020−12025.
(34) Huey, R., and Morris, G. M. (2009) *Using Autodock 4 with AutoDock Tools: A Tutorial*, The Scripps Research Institute, La Jolla, CA.
(35) Morris, G. M., Goodsell, D. S., Pique, M. E., Lindstrom, W., Huey, R., Forli, S., Hart, W. E., Halliday, S., Belew, R., and Olson, A. J. (2009) *User Guide Autodock 4.2*, The Scripps Research Institute, La Jolla, CA.
(36) Yeh, L. C., Betchel, K. P., and Lee, J. C. (1998) Inhibition of BMP receptor synthesis by antisense oligonucleotides attenuates OP-1 action in primary cultures of fetal rat calvaria cells. *J. Bone Miner. Res. 13*, 1870−1897.
(37) Manson, A., Whitten, S. T., Ferreon, J. C., Fox, R. O., and Hilser, V. J. (2009) Characterizing the role of ensemble modulation in mutation-induced changes in binding affinity. *J. Am. Chem. Soc. 131*, 6785−6793.
(38) Liu, T., Whitten, S. T., and Hilser, V. J. (2007) Functional residues serve a dominant role in mediating the cooperativity of the protein ensemble. *Proc. Natl. Acad. Sci. U.S.A. 104*, 4347−4352.
(39) Whitten, S. T., Garcia-Moreno, E. B., and Hilser, V. J. (2005) Local conformational fluctuations can modulate the coupling between proton binding and global structural transitions in proteins. *Proc. Natl. Acad. Sci. U.S.A. 102*, 4283−4287.
(40) Hilser, V. J., Garcia-Moreno E., B., Oas, T. G., Kapp, G., and Whitten, S. T. (2006) A statistical thermodynamic model of the protein ensemble. *Chem. Rev. 106*, 1545−1558.